The Astrophysical Journal, 659:848–857, 2007 April 10
© 2007. The American Astronomical Society. All rights reserved. Printed in U.S.A.

VALIDATION OF TIME-DISTANCE HELIOSEISMOLOGY BY USE OF REALISTIC SIMULATIONS OF SOLAR CONVECTION

Junwei Zhao, Dali Georgobiani, and Alexander G. Kosovichev
Hansen Experimental Physics Laboratory, Stanford University, Stanford, CA 94305-4085

David Benson[1] and Robert F. Stein
Physics and Astronomy Department, Michigan State University, East Lansing, MI 48824

and

Åke Nordlund
Niels Bohr Institute, Copenhagen University, DK-2100 Copenhagen Ø, Denmark
Received 2006 November 7; accepted 2006 December 19

ABSTRACT

Recent progress in realistic simulations of solar convection have given us an unprecedented opportunity to evaluate the robustness of solar interior structures and dynamics obtained by methods of local helioseismology. We present results of testing the time-distance method using realistic simulations. By computing acoustic wave propagation time and distance relations for different depths of the simulated data, we confirm that acoustic waves propagate into the interior and then turn back to the photosphere. This demonstrates that in numerical simulations properties of acoustic waves (*p*-modes) are similar to the solar conditions, and that these properties can be analyzed by the time-distance technique. For surface gravity waves (*f*-modes), we calculate perturbations of their travel times caused by localized downdrafts and demonstrate that the spatial pattern of these perturbations (representing so-called sensitivity kernels) is similar to the patterns obtained from the real Sun, displaying characteristic hyperbolic structures. We then test time-distance measurements and inversions by calculating acoustic travel times from a sequence of vertical velocities at the photosphere of the simulated data and inferring mean three-dimensional flow fields by performing inversion based on the ray approximation. The inverted horizontal flow fields agree very well with the simulated data in subsurface areas up to 3 Mm deep, but differ in deeper areas. Due to the cross talk effects between the horizontal divergence and downward flows, the inverted vertical velocities are significantly different from the mean convection velocities of the simulation data set. These initial tests provide important validation of time-distance helioseismology measurements of supergranular-scale convection, illustrate limitations of this technique, and provide guidance for future improvements.

Subject headings: convection — Sun: helioseismology — Sun: oscillations

1. INTRODUCTION

Time-distance helioseismology, along with other helioseismology techniques, is an important tool for investigating the solar interior structure and dynamics. Since it was first introduced by Duvall et al. (1993) this technique has been used to derive the interior structure and flow fields of relatively small scales, such as supergranulation and sunspots (e.g., Kosovichev 1996; Kosovichev & Duvall 1997; Kosovichev et al. 2000; Gizon et al. 2000; Zhao et al. 2001; Couvidat et al. 2004), and also at the global scale, such as differential rotation and meridional flows (e.g., Giles et al. 1997; Chou & Dai 2001; Beck et al. 2002; Zhao & Kosovichev 2004). These studies, together with other local helioseismology techniques (e.g., Komm et al. 2004; Basu et al. 2004; Braun & Lindsey 2000), have opened a new frontier in studies of solar subsurface dynamics. Meanwhile, modeling efforts of time-distance helioseismology have also been carried out to interpret the time-distance helioseismology measurements and provide sensitivity kernels used in inversions of the solar interior properties (e.g., Gizon & Birch 2002; Jensen & Pijpers 2003; Birch et al. 2004).

However, despite the observational and modeling efforts it is difficult to evaluate the accuracy or even correctness of the local helioseismological results because the interior of the Sun is inaccessible to direct observations. Still, there are a couple of approaches that help to evaluate the inverted results. One of these is to compare the inverted solar interior structures with models, e.g., comparing the subsurface flow fields below sunspots (Zhao et al. 2001) with results of sunspot models (Hurlburt & Rucklidge 2000). Another approach is to compare the flow maps obtained by different helioseismological techniques, e.g., comparing *f*-mode time-distance measurements of near-surface flows with measurements of flows obtained by the ring-diagram technique (Hindman et al. 2004). However, the first approach is only qualitative, and although the second approach is somewhat quantitative there is a possibility that different helioseismological techniques may provide similar incorrect results because they do not account for turbulence and rapid variability of the subsurface flows.

A convincing way to validate time-distance helioseismology is to perform measurements and inversions on a set of realistic large-scale numerical simulation data, which not only model the turbulent convective motions of various scale in and beneath the solar photosphere but also carry acoustic oscillation signals generated by the motions. These simulations have the following properties: the spatial resolution is comparable to or better than that in typical helioseismological observations, the size of the computational domain is larger than a typical supergranule, the temporal resolution is sufficiently high to capture useful acoustic oscillation signals, and the time duration is long enough to extract

[1] Current address: Department of Mechanical Engineering, Kettering University, Flint, MI 48504.

acoustic signals with a satisfactory signal-to-noise ratio. The helioseismology techniques can then be evaluated by comparing the inverted interior results obtained from analyzing surface acoustic oscillations with the interior structures directly from the numerical simulation.

In this paper, we use realistic three-dimensional simulations in solar convections by Benson et al. (2006), which were based on the work of Stein & Nordlund (2000). These simulations have enabled us to directly evaluate the validity of time-distance helioseismology measurements of the quiet-Sun convection. In a previous paper, Georgobiani et al. (2007; hereafter Paper I) analyzed the oscillation properties of these simulations and found that the power spectrum is similar to the power spectrum obtained from real Michelson Doppler Imager (MDI) high-resolution Dopplergrams. Their analysis of time-distance diagrams also showed that the simulated data had time-distance relations similar to those of the real Sun. Furthermore, the near-surface *f*-mode analysis using the simulated data gave surface structures similar to both those obtained from local correlation tracking and those actually in the simulation. Thus, this set of realistic simulations of solar convection by Benson et al. (2006) is quite suitable for detailed *p*-mode time-distance studies and allows us to evaluate the accuracy of inverted time-distance results.

In this paper we introduce the simulated data in § 2. Then we check the properties of acoustic propagation in the interior regions of the simulated data and make sure that acoustic signals seen at the surface do carry information from the interior. We present these analyses in § 3. In § 4 we calculate the surface sensitivity kernel from this data set. Then in § 5 we carry out *p*-mode time-distance measurements and inversions to infer interior flow fields and compare our inverted results with the corresponding simulation data. Discussion follows in § 6.

2. NUMERICAL SIMULATION DATA

The numerical simulation data we use in this paper are results of the computation of multiscale solar convection in the upper solar convection zone and photosphere (Benson et al. 2006) using a three-dimensional compressible, radiative-hydrodynamic code, which employs LTE, nongray radiative transfer, and a realistic equation of state and opacities (Stein & Nordlund 2000).

In the space domain, the simulated data span 48 Mm $\times$ 48 Mm horizontally and 20 Mm vertically, with a horizontal spatial resolution of 96 km pixel^{-1} and a varying vertical spatial resolution from 12 to 75 km pixel^{-1}. In the time domain the data were saved every 10 s, but in practice we used only every third snapshot, i.e., every 30 s, because the 10 s temporal resolution provides an acoustic frequency range far beyond the typical solar oscillation frequencies. The whole simulation used in this analysis lasts 511 minutes. The acoustic k-ω diagram and the time-distance diagram obtained from this simulated data set in the photosphere can be found in Paper I. In this paper and Paper I, the level of the height of formation of the center of the λ676.78 nm Ni line observed by *SOHO* MDI is taken as the 0 Mm level for the convenience of description in the following text. It is 200 km above continuum optical depth unity.

Figure 1 presents a snapshot of vertical velocity from the simulation, showing three horizontal slices taken at depths of 0, 8, and 16 Mm, and one vertical slice. One can see small-scale granular structures in the photosphere, with downdraft lanes at the granular boundaries and relatively weaker upflows inside granules. Several megameters below the photosphere, small granular structures disappear and are replaced by larger scale structures, but with similar flow patterns, downdrafts at boundaries, and upward flows inside the structure.

3. PROPAGATION PROPERTIES OF ACOUSTIC WAVES

It is already clear that at the photospheric level the simulations carry acoustic oscillations similar to those of the real solar observations, as demonstrated in Paper I. Since the goal of this paper is to evaluate time-distance helioseismology in the interior by use of *p*-mode analysis, it would be useful and necessary to check whether the proper acoustic oscillations exist in the interior of the simulated convection, and whether acoustic waves propagate inside properly.

The solar acoustic waves are excited stochastically by multiple random sources in the upper convection zone. In time-distance helioseismology, coherent wave signals are constructed by calculating a cross-correlation function of oscillations observed at locations $\boldsymbol{r}_1$ and $\boldsymbol{r}_2$, separated by distance Δ and for time lag τ:

$$C(\Delta,\ \tau) = \int_0^T f(\boldsymbol{r}_1,\ t) f(\boldsymbol{r}_2,\ t+\tau)\, dt, \tag{1}$$

where $f(\boldsymbol{r},\ t)$ is the oscillation signal at location $\boldsymbol{r}$, Δ is distance between $\boldsymbol{r}_1$ and $\boldsymbol{r}_2$, and T is the duration of the whole sequence. The cross-correlation for each distance is obtained by averaging numerous cross-correlations calculated between pairs of pixels, which are a given distance, Δ, apart.

The time-distance diagram, as shown in Figure 2 in Paper I, and many other time-distance diagrams published in literature are actually a collection of computed cross-correlations with continuous time lags, displayed as a function of acoustic wave travel distance. According to the conjecture of Rickett & Claerbout (2000), the cross-covariance function may be considered as a signal from a point surface source of some particular spectral properties. Nearly all the previously published time-distance diagrams were obtained at the photospheric level, as no observations or simulations below the photosphere were available before.

With the availability of three-dimensional convection simulation, we are now capable of computing the time-distance diagrams at different depths beneath the photosphere by cross-correlating acoustic signals at a desired depth with signals in the photosphere and following the equation

$$C(\Delta,\ \tau,\ d) = \int_0^T f(\boldsymbol{r}_1,\ 0,\ t) f(\boldsymbol{r}_2,\ d,\ t+\tau)\, dt, \tag{2}$$

where $f(\boldsymbol{r},\ d,\ t)$ is the oscillation signal at horizontal location $\boldsymbol{r}$, and at the depth of d and time t. Because of the great computational burden, in practice such computations are performed in the Fourier domain. The time-distance diagram at a depth d shows the time it takes the acoustic wave to travel from a point at the surface to a point at the depth d and a horizontal distance Δ away.

We have computed nearly 100 such time-distance diagrams at every fifth depth of the simulated data, since the original data have 500 vertical mesh points, but some of these mesh points are above the photosphere and not used in computing these diagrams. Several selected depths are presented in Figure 2. The diagram at a depth of 0 Mm is actually the time-distance diagram for the photosphere. The evolution of acoustic signals with time and the propagation along horizontal distance are clearly seen from 0 Mm to a depth of 8 Mm, approximately. The time-distance diagrams match very well with the expected time-distance relationships derived from the ray theory, as indicated by the dashed lines in each diagram. Below 8 Mm, the signals are not so clear as above.

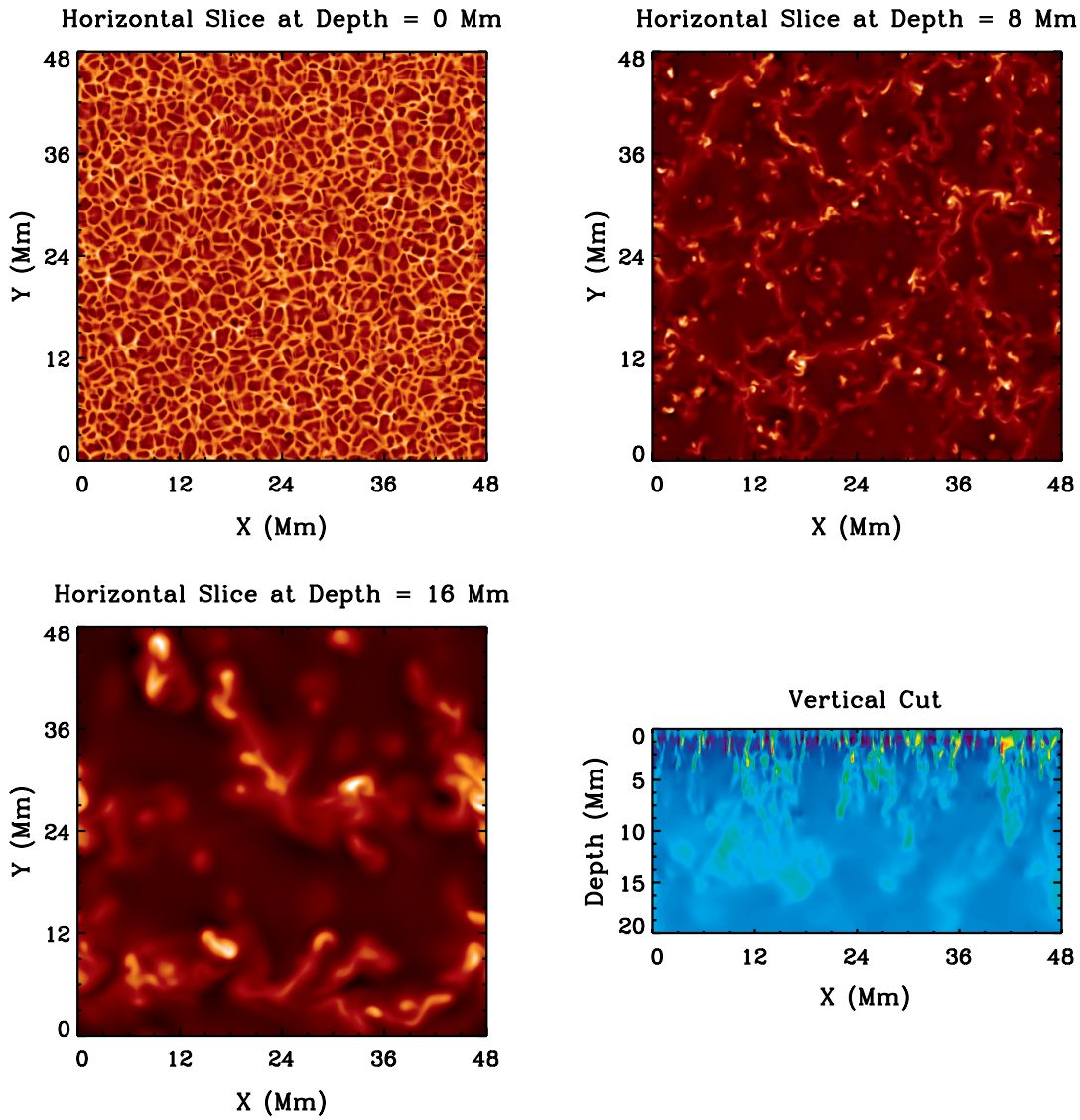

FIG. 1.— Snapshots of the vertical component of velocity taken from the numerical simulation of solar convection, showing three horizontal slices taken at depths of 0, 8, and 16 Mm, and a vertical slice, respectively. In the vertical cut, green and yellow represent downflows, while blue and dark regions represent upflows. In the horizontal slices, bright regions show downflows, and dark regions show upflows.

The two-dimensional time-distance diagrams for different depths can be represented as a three-dimensional data cube with two spatial dimensions, horizontal distance Δ and depth d, and time τ. It is interesting to display the spatial images as a time sequence showing acoustic waves propagating from the surface into the interior. Some selected images of this sequence are displayed in Figure 3. The left side of each image is symmetrized with the right side. In order to better show the weak signals in the deeper regions, the signals near the surface are intentionally saturated.

As can be seen from the time-distance diagram at the depth of 0 Mm in Figure 2, the acoustic waves travel like a wave packet, with an oscillation period of 5 minutes or so, and a width of about 17 minutes (also see Duvall et al. 1997). In Figure 3, at $\tau = 1$ minute, one can see a very small blue feature at the top; this is considered to be the first negative oscillation in the wave packet. With the evolution of time the blue feature, i.e., the wave front, expands in size and propagates into the interior. It is followed by a signal of the opposite sign, a red feature, which is initiated at $\tau = 5$ minutes. We note that at some moments of the evolution, the wave fronts become open at their horizontal central region. In the upper 10 Mm or so, the general circular wave shapes are often kept well, but below 10 Mm the wave structure is often irregular and noisy. Also, it looks like some signals, although weak, are reflected back from the bottom boundary.

It is curious that the central part of the waves is open. This may result from the following reason: because the horizontal span of the simulation domain is only 48 Mm, the simulated data cannot carry any acoustic wave modes that have a first-bounce travel distance longer than 48 Mm. Clearly, the modes that travel a longer first-bounce distance contribute most of the signal at the central part of the wave fronts. A simple estimate of the turning depth of the acoustic waves corresponding to a first-bounce travel distance of 48 Mm is approximately 15 Mm. This is roughly in agreement with the images in Figure 3, in which no clear signals deeper than 15 Mm can be seen.

Despite the curious open structures at the central part of wave fronts, the noise outside the wave features, and some reflected signals from the bottom, it is quite clear the waves are substantial, clear, and in nice agreement with the theoretical expectations. The constructed wave propagation clearly shows that the

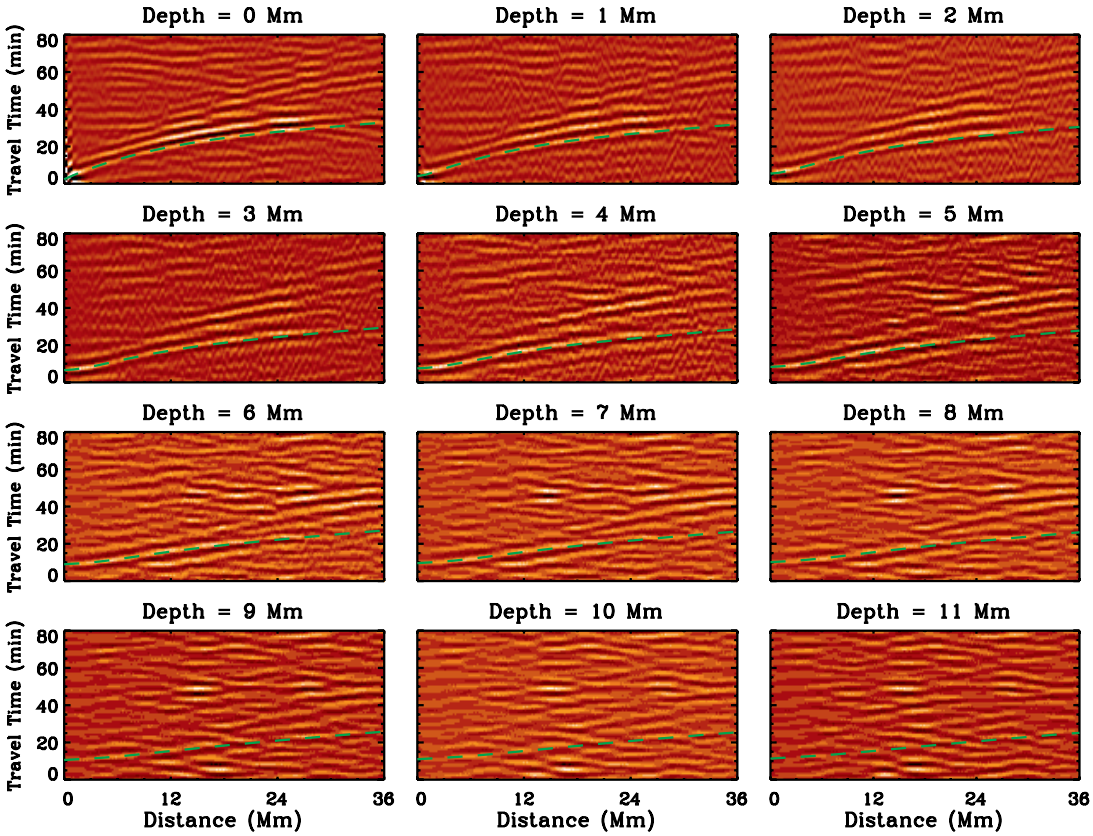

FIG. 2.—Time-distance diagrams, $C(\Delta, \tau, d)$, calculated from the simulated data at several selected depths, showing the ridges corresponding to the relationships between acoustic travel times and distances at different depths after an acoustic wave is initiated at the depth of 0 Mm. Green dashed lines in each diagram indicate expectations of the time-distance relationships based on the ray theory.

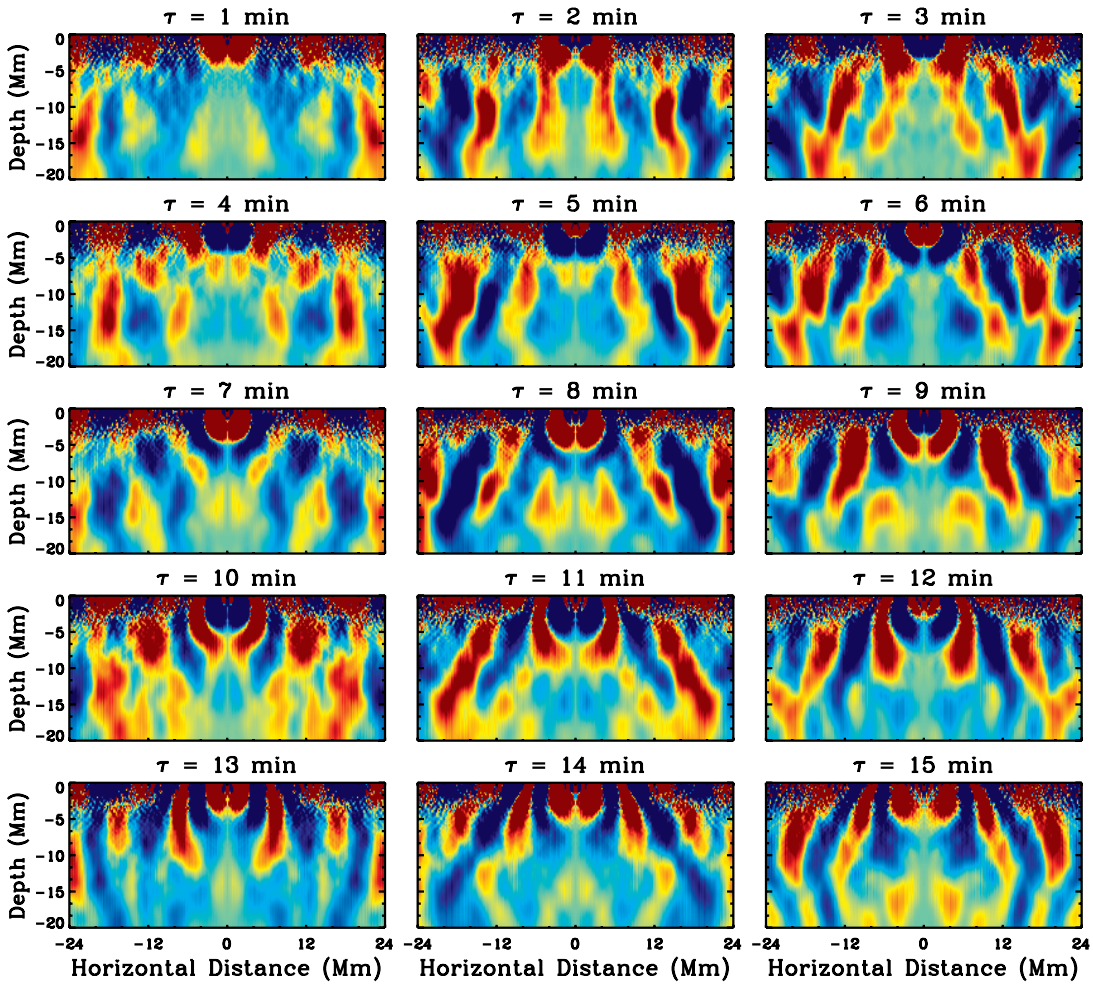

FIG. 3.—Selected snapshots showing the propagation of acoustic waves into the interior and reflecting back to the surface. See the text for details.

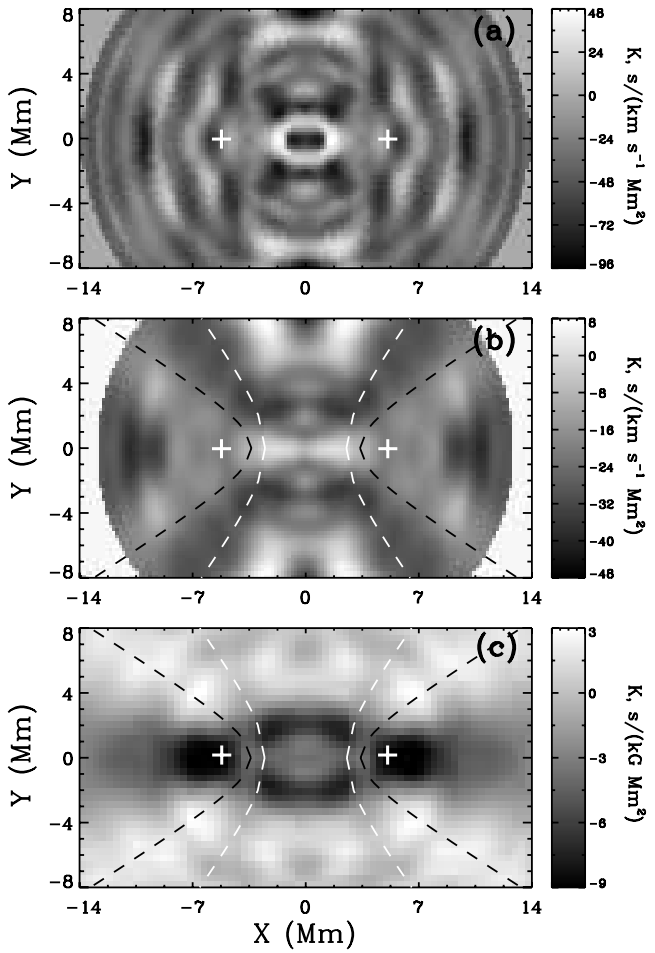

FIG. 4.—(*a*) Sensitivity kernel measured around downdraft locations from the simulated data using *f*-modes. (*b*) Sensitivity kernel obtained by smoothing the kernel in (*a*). (*c*) Sensitivity kernel measured around small magnetic elements from *SOHO* MDI observations (adapted from Duvall et al. 2006). The black and white dashed hyperbolas in (*b*) and (*c*) indicate the locations of two hyperbolic structures observed in (*c*). The white plus signs in each panel indicate the locations of observation points.

waves are refracted back to the surface from different turning points, as expected from linear helioseismology theories. It is a great success of the time-distance technique that it is capable of retrieving acoustic wave propagation in the deep, very turbulent interior, and it is also a great success for the simulations that they reproduce the basic properties of acoustic waves in the solar interior. Therefore, we conclude that this simulation data set is quite suitable for testing the *p*-mode time-distance analysis, while keeping in mind that the deepest acoustic wave probe depth in these simulations is shallower than 15 Mm.

4. PROPAGATION OF SURFACE GRAVITY WAVES: SCATTERING AND SENSITIVITY KERNELS

The sensitivity functions (or kernels) represent perturbations of travel times to small localized features on the Sun. To evaluate the potential for using surface gravity waves (*f*-modes) in the simulations for testing the *f*-mode diagnostics, we have calculated empirical sensitivity functions following the recent work of Duvall et al. (2006). Their work has offered us not only another method for checking the helioseismic reasonableness of the simulated data, but also a meaningful approach to compute the sensitivity kernels that is potentially useful for time-distance inversions.

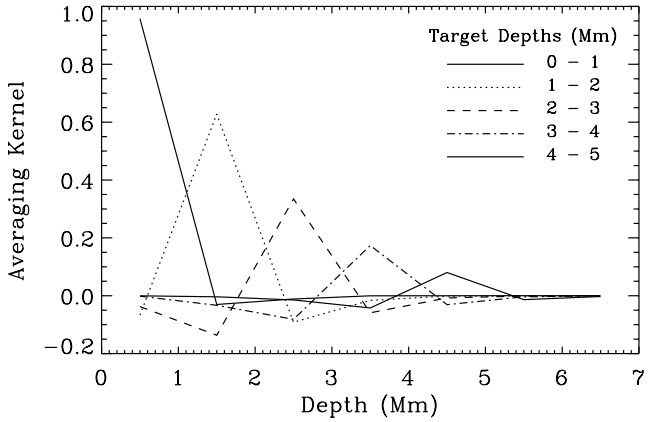

FIG. 5.—Averaging kernels for the selected target depths. Note that each point is plotted at the middle of its corresponding depth interval.

Duvall et al. (2006) computed the sensitivity kernels for *f*-modes by measuring travel-time variations around some small magnetic elements from real MDI observations. They found elliptic and hyperbolic structures in the kernels, which are similar to the structures modeled by Gizon & Birch (2002) and attributed to wave-scattering effects. Because of wave scattering, the travel times are sensitive not only to perturbations in the region of wave propagation between two points but also in some areas away from the path, along hyperbola-shaped regions. They concluded that their measurements demonstrated that the Born approximation was suitable for deriving time-distance inversion kernels, and that the wave-scattering effect is important and has to be included in the derivation of the sensitivity kernels for helioseismic inversions.

Here we try to check whether a sensitivity kernel with similar hyperbolic structures can be obtained from the numerical simulations, and thus whether the wave scattering is properly modeled in the simulated data.

Since there are no magnetic elements in the current simulation data set, we select areas with strong downdrafts as the features to calculate the travel-time sensitivity kernels. We average the vertical velocity over the whole time sequence of 511 minutes, and select 50 small areas that have the strongest downward flows. We set these 50 areas as the central features to compute the kernels. We then follow the procedure described as "feature method" in Duvall et al. (2006) and compute travel-time variations around these selected downdrafts areas. We follow every step described in this paper, except that we use a longer time series in our computations, and that we use the Gabor wavelet fitting to measure the wave travel times. Although we have only one data sequence, and just 50 selected downdraft areas available for averaging (unlike a number of observational data sets and thousands of magnetic elements in the Duvall et al. [2006] paper), we were able to obtain the sensitivity kernels with a reasonable signal-to-noise ratio. Still, we had to do additional spatial averaging to recover the wave-scattering structures.

Figure 4 presents the results of our measurements before (Fig. 4*a*) and after (Fig. 4*b*) boxcar smoothing. There are some small-scale black and white patches in the measured original travel-time variations, and large-scale structures are not quite clear, although such structures do exist. Such small-scale structures are not seen in the kernels obtained from real observations; this may be possibly caused by the fact that the numerical simulation data have a much higher spatial resolution than the real observations, and thus our measurements could pick up some small-scale signals that are not resolved in the observational data.

TABLE 1
CORRELATION COEFFICIENTS BETWEEN INVERTED RESULTS AND SIMULATED DATA AT DIFFERENT DEPTHS

Depth (Mm)	v_x	v_y	Divergence	v_z
0–1	0.72 (0.72)	0.64 (0.64)	0.56 (0.56)	−0.72
1–2	0.85 (0.87)	0.76 (0.76)	0.89 (0.91)	−0.72
2–3	0.87 (0.92)	0.74 (0.83)	0.78 (0.84)	−0.29
3–4	0.74 (0.84)	0.37 (0.53)	0.36 (0.50)	0.34
4–5	0.18 (0.51)	0.25 (0.62)	−0.35 (−0.11)	0.32

NOTE.—The numbers shown in parentheses are correlation coefficients after the simulated data are convolved with the inversion averaging kernels.

In addition, the convective structures we use for such measurements are much less stable than the real magnetic elements, which may also contribute some noises to the measurements.

To get a better signal-to-noise ratio for large-scale structures, we applied a boxcar smoothing to the original measurements and obtain the result shown in Figure 4*b*. The hyperbolic dark and light features appear quite clearly, similar to the sensitivity kernel measured from magnetic elements of real observations, although the locations have slight offsets, as indicated by the dashed lines. However, the details are not comparable, because our sensitivity kernel is measured around large downdrafts areas, but not for magnetic elements as in Figure 4*c*.

It is important that the hyperbolic structures are found in the *f*-mode sensitivity kernels obtained from the simulated data, because this demonstrates that the wave-scattering effect is reproduced in the numerical simulation of convection. However, at present it is difficult to use the empirical sensitivity kernels in time-distance inversions because the measured kernels, such as the one shown in Figure 4, may depend on various factors at the downdraft locations, for instance, not only the vertical component of flow, but also the converging flows that are often associated with the downdrafts. This issue requires further investigation.

5. TIME-DISTANCE HELIOSEISMOLOGY TEST FOR SUBSURFACE FLOWS

To test the current time-distance helioseismology procedure we measured travel times of acoustic waves using only the vertical velocity at the photospheric level from the simulated data,

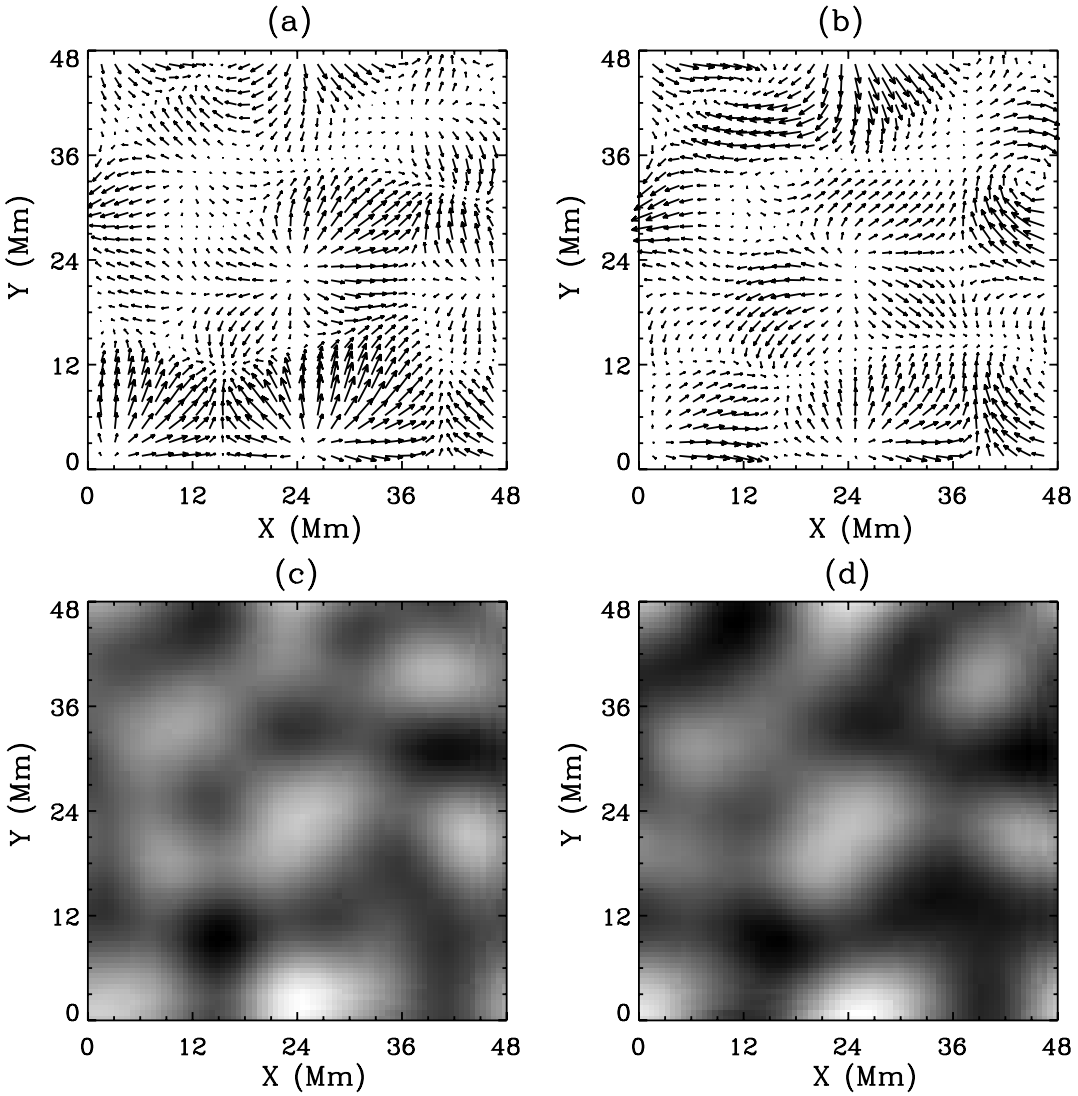

FIG. 6.— Comparison of the inverted horizontal flow fields with the simulated data at a depth of 1–2 Mm: horizontal flow fields from (*a*) the simulations and (*b*) the inversions, and a divergence map from (*c*) simulation (*d*) and inversion. Both vector flow fields and both divergence maps are displayed with the same scales. The longest arrow corresponds to 300 m s^{-1}.

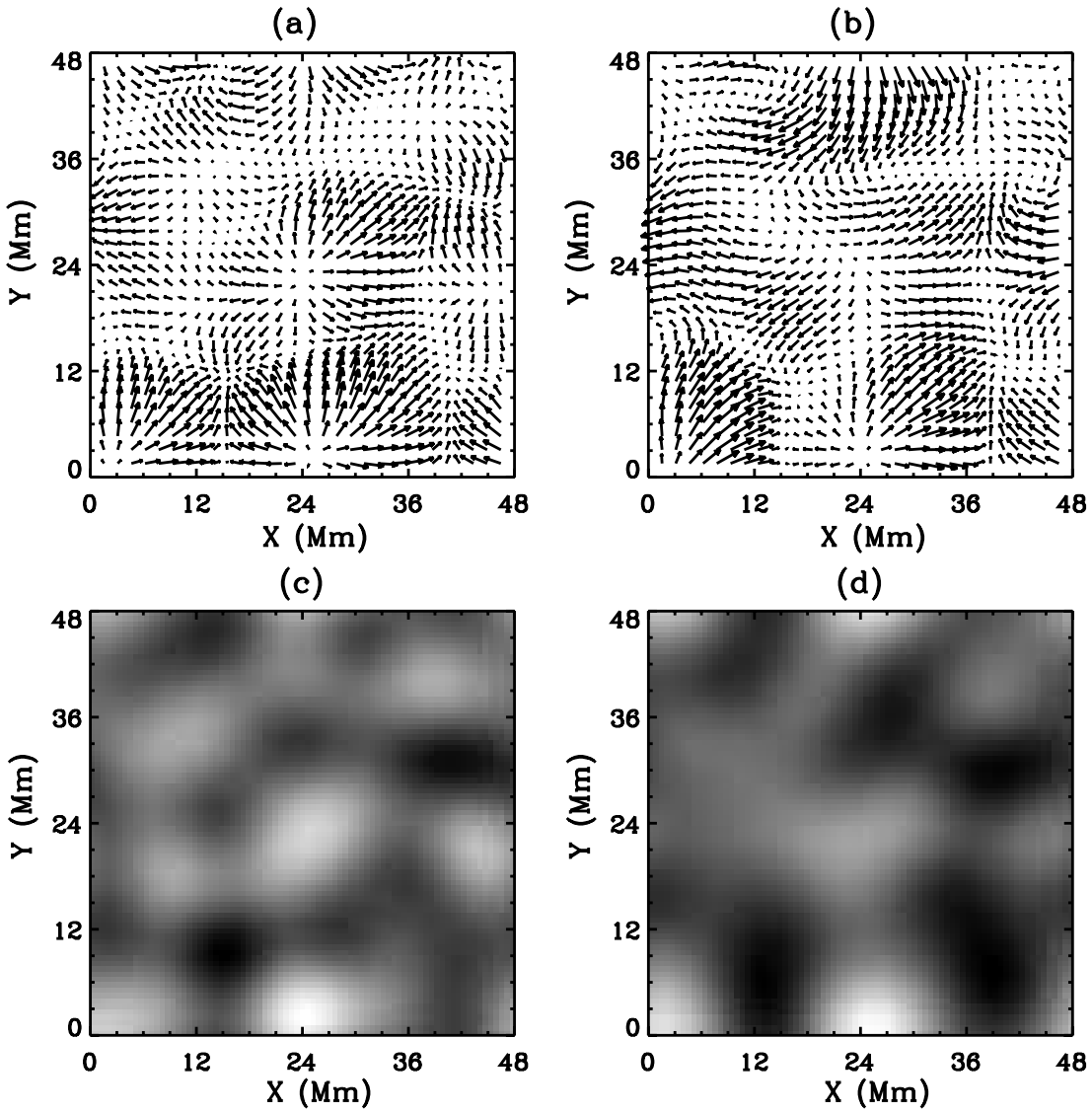

FIG. 7.—Same as Fig. 6, but at a depth of 2–3 Mm.

then inferred the three-dimensional velocities in the interior by using an inversion procedure based on a ray approximation (Kosovichev & Duvall 1997; Kosovichev et al. 2000; Zhao et al. 2001), and finally compared the inversion results with the averaged interior velocities from the simulations. Following the typical *p*-mode time-distance measurement schemes (e.g., Zhao et al. 2001), we select the following seven annulus radii to perform our measurements: 8.64–10.37, 10.56–12.29, 12.48–14.21, 14.40–16.13, 16.32–18.05, 18.24–19.97, and 20.16–21.89 Mm. The greatest annulus is a little smaller than half of the horizontal span of the simulated data. In order to evaluate the previous inversion results, the inversions here employ the ray-approximation kernels.

To evaluate the inverted time-distance results, we compare our inversion results for flows with the actual flow fields directly from the simulated data. The inverted results are often given as averages of some depth ranges, for instance, 1–2 Mm in Figure 6. Hence, the simulated data are also averaged arithmetically in the same depth interval over the 511 minutes. For each target depth, the averaging kernels from the inversion are three-dimensional, and Figure 5 only presents a one-dimensional curve corresponding to the central point. In addition to the direct comparisons, it is interesting to convolve the three-dimensional averaging kernels with the three-dimensional simulated velocities and see how the resultant velocities compare with the inverted velocities. In the following, we present results from the direct comparison, but give the correlation coefficients of both comparisons in Table 1.

5.1. *Horizontal Flow Fields*

Figures 6, 7, and 8 present the inversion results for the horizontal flow components in three layers: 1–2, 2–3, and 4–5 Mm deep. Comparing the horizontal vector flows, as well as the divergence map computed from the horizontal flows, we find that at the depth of 1–2 Mm the inversion results agree quite well with the time-averaged simulation results. The results reveal areas of strong flow divergence, which have a typical size of solar supergranulations. This is in good agreement with the results obtained by the time-distance analysis of *f*-modes and by a correlation tracking method, which are both presented in Paper I. These divergent areas are nearly in one-to-one correspondence between the inverted results and the simulated data, with similar magnitudes as well. It should be pointed out that the flow maps for the simulated data are displayed after applying a low-pass filtering to only keep structures that have a wavenumber smaller than

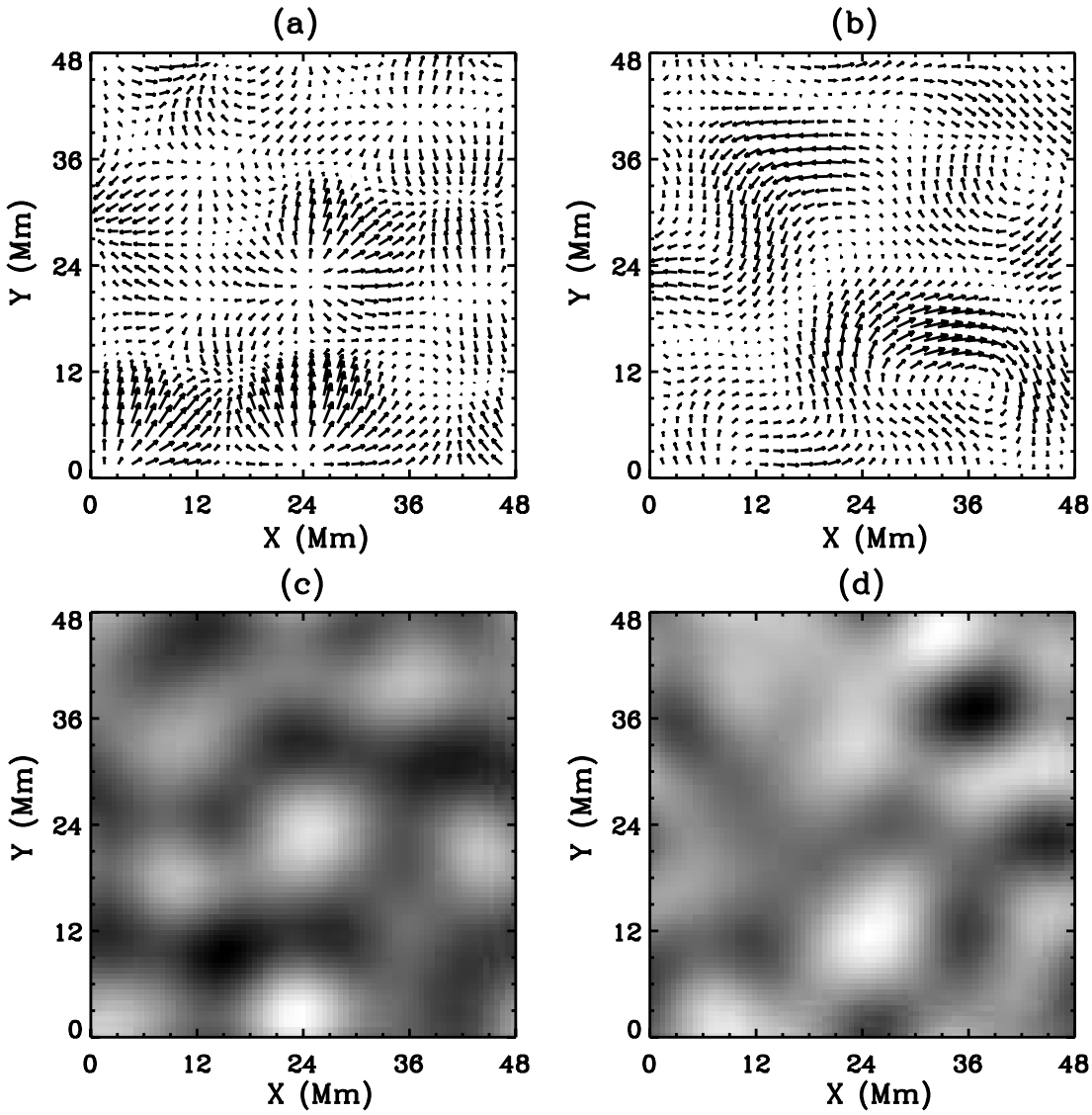

FIG. 8.—Same as Fig. 6, but at a depth of 4–5 Mm.

0.06 Mm^{-1}, in order to better match the time-distance computational procedures, which undergo filtering and smoothing during measurements and inversions.

As the inverted area deepens, the correlation between the inverted results and the simulated data gradually worsens. At the depth of 2–3 Mm one can still see those divergent flow patterns in both data, but clearly not as clearly as at the depth of 1–2 Mm. However, at the depth of 4–5 Mm and deeper, the inverted horizontal flows show no clear correlation with the simulated data.

Table 1 presents the correlation coefficients between the inverted results and the simulated data at different depths in two horizontal velocity components, the divergences that are computed from the horizontal components, and the vertical velocity (see the next section), separately. It is clear that the shallow regions often have better correlations than the deeper regions, except for the vertical velocity. It is curious but not clear why the two horizontal components have correlation coefficients that differ so much, with the north-south direction often worse than the east-west direction. A similar east-west and north-south asymmetry in time-distance results was also found when comparing with local correlation tracking results (Švanda et al. 2007). In addition, the correlation of the divergence maps also differs from that of the horizontal components. It is worthwhile to point out that after the simulated data are convolved with the inversion averaging kernels, the correlation coefficients are generally improved, significantly in the deeper areas.

5.2. *Vertical Flow Fields*

It is often the case in both real observations and numerical simulations that in the photosphere the vertical velocity is significantly smaller than the horizontal velocity of the same depth, due to the strong density stratification in the upper solar convection zone. And often, near the surface, the downward flows concentrate in very narrow lanes among boundaries of granules or supergranules. These properties make it more difficult to infer vertical velocities by the local helioseismology techniques, which often involves large-area smoothing, because the small-magnitude vertical velocity in small areas can be easily smeared out.

Figure 9 presents results of time-distance inverted results of vertical flows, along with the averaged vertical velocities from simulated data at the corresponding depths. At the depth of 1–2 Mm the inverted vertical velocities basically have opposite

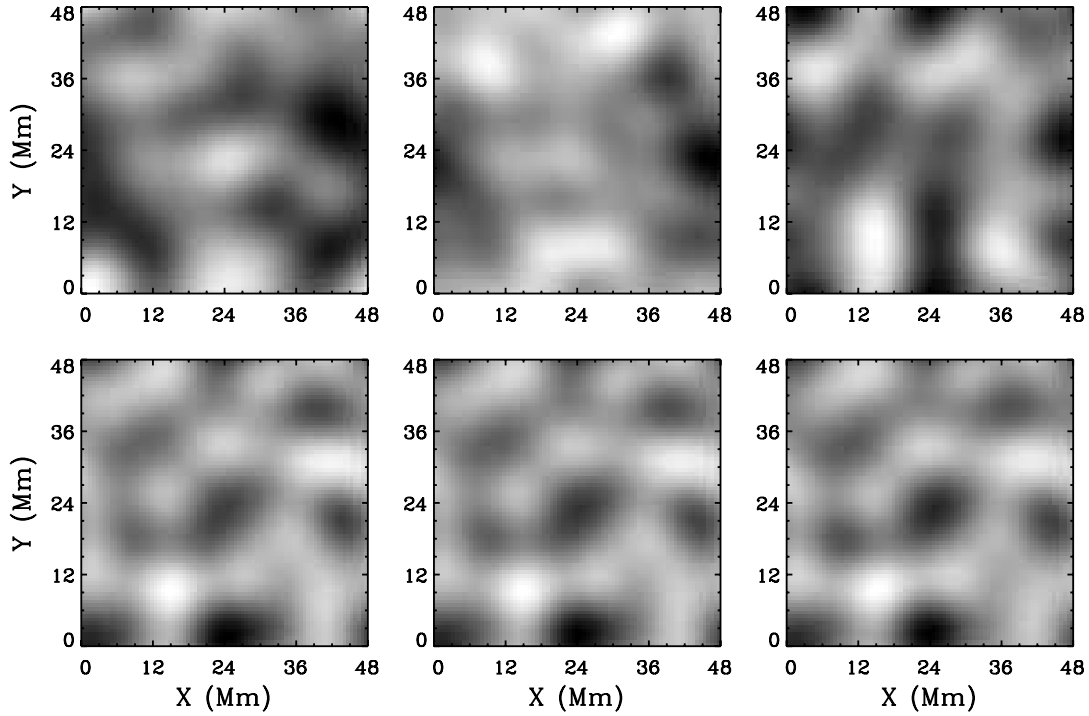

FIG. 9.—Comparison of the inverted vertical flows with the simulated data. The top panels show the vertical velocities from inversion at the target depths of, from left to right, 1–2, 2–3, and 4–5 Mm. The bottom panels show the simulated vertical flows averaged for the corresponding depth ranges. Dark regions show upflows, and light regions show downflows. The velocity range is from −150 to 150 m s^{-1}.

signs to the simulated velocities. For the other two depths, no clear correlation or anticorrelation is seen. As also presented in Table 1, the correlation coefficients show that at shallow depths inverted vertical flows are in anticorrelation with the simulated data, while at deeper depths the correlations are positive but weak. It seems that the inversions for the vertical flow fields are completely unsuccessful. This discrepancy is not only due to the small magnitude of vertical velocities, but is also caused by the cross-talk effects discussed in the next section.

6. DISCUSSION

The realistic simulation of solar convection obtained by Benson et al. (2006) gives us an unprecedented opportunity to evaluate the time-distance helioseismology technique and some other local helioseismology approaches.

By computing the time-distance diagrams at different depths, as shown in Figures 2 and 3, we have confirmed that there are acoustic waves propagating in the interior in the simulated data with properties similar to those expected from the helioseismology theory. Although there are some unexplained correlated signal noises, bottom reflections, and open structure at the center of the wave front, these do not affect our time-distance analysis in shallow regions below the surface. The longest annulus used in our analysis is about 21 Mm, which probes to a depth of approximately 6.5 Mm according to ray theory, shallow enough not be affected by those unexplained factors in the simulations. Our measurements of the *f*-mode sensitivity kernel near the surface, shown in Figure 3, have demonstrated that the convection simulation data have wave-scattering properties similar to the real solar observations. These analyses demonstrate that the simulated data have the wave properties that are necessary for time-distance helioseismology analysis.

Using very turbulent convection data at the photospheric level and the time-distance technique based on a ray approximation, we were able to derive the internal flow fields, which are in nice correlation with the simulation results in shallow regions. It is not surprising that the time-distance inversions cannot resolve properties well at greater depths, which was already demonstrated by some artificial data tests (e.g., Kosovichev 1996; Zhao et al. 2001). It is believed that the reliability of inversion results highly depends on the number of ray paths passing through that area, whereas deeper areas have fewer ray paths passing through and less information brought up to the surface. In addition, it should be recognized again that the horizontal scale size of 48 Mm limits the deepest ray path penetration at a depth of approximately 15 Mm, and our longest annulus radius once again limits our deepest probe to a depth of 6.5 Mm or so. Therefore, it is quite reasonable that our inversions give acceptable results until a depth of only 4 Mm or so.

It is also not surprising to see the failure of vertical flows in inversions. Certainly, the small magnitudes of vertical velocity may be one reason. However, we believe that the main reason for the failure is due to the cross-talk effects, as already demonstrated by use of some artificial tests (Zhao & Kosovichev 2003). The divergence inside supergranules speeds up outgoing acoustic waves in the same way downdrafts do, and similarly, the convergence at boundaries of supergranules slows down outgoing waves from this region in ways similar to what upflows do. The time-distance inversions cannot distinguish the divergence (or convergence) from downward (or upward) flows, especially when the vertical flow is small in magnitude. Although it is believed that some additional constraints, e.g., mass conservation, may help the inversion in resolving vertical flows, the current inversion technique of time-distance restricts itself to using pure helioseismological measurements. This set of simulated data may give us a very good test ground for the future development of vertical velocity inversion codes.

Still, inversions in this study use the ray-approximation kernels in order to evaluate the old results published previously that used such kernels. With the availability of Born approximation kernels

(Birch et al. 2004), it would be very interesting to test such kernels with this kind of analysis on the current simulated data set, although some previous experiments (Couvidat et al. 2004) showed that inversion results based on two different kernels do not differ much. It is expected that the Born kernel may give better results in deeper areas, but may not be able to solve the vertical velocity problem caused by the cross-talk effects. New time-distance helioseismology schemes are probably required for the solution.

The numerical simulation of solar convection gives us an opportunity to evaluate the time-distance technique in quiet solar regions. However, it would be especially interesting if we could test this helioseismology technique in a magnetized region, as the simulations of magnetoconvection (e.g., Stein & Nordlund 2006; Schüssler & Vögler 2006) are extended in both spatial and temporal scales to meet the helioseismological measurement requirements. For instance, we can evaluate the accuracy of the inferred sunspot structures and flow fields (Kosovichev et al. 2000; Zhao et al. 2001) and evaluate various magnetic field effects based on such numerical simulations.

We thank Tom Duvall for providing us data making Figure 4*c*, and Takashi Sekii for insightful comments on the interpretation of interior wave propagations. We also thank an anonymous referee for suggestions that improved the quality of this paper. The numerical simulations used in this work were made with support by NASA grants NNG04GB92G and NAG5 12450, NSF grants AST 02-05500 and AST 06-05738, and by grants from the Danish Center for Scientific Computing. The simulations were performed on the Columbia supercomputer of the NASA Advanced Supercomputing Division.

REFERENCES

Basu, S., Antia, H. M., & Bogart, R. S. 2004, ApJ, 610, 1157
Beck, J. G., Gizon, L., & Duvall, T. L., Jr. 2002, ApJ, 575, L47
Benson, D., Stein, R., & Nordlund, Å. 2006, in ASP Conf. Ser. 354, Solar MHD Theory and Observations: A High Spatial Resolution Perspective, ed. H. Uitenbroek, J. Leibacher, & R. F. Stein (San Francisco: ASP), 92
Birch, A. C., Kosovichev, A. G., & Duvall, T. L., Jr. 2004, ApJ, 608, 580
Braun, D. C., & Lindsey, C. 2000, Sol. Phys., 192, 307
Chou, D.-Y., & Dai, D.-C. 2001, ApJ, 559, L175
Couvidat, S., Birch, A. C., Kosovichev, A. G., & Zhao, J. 2004, ApJ, 607, 554
Duvall, T. L., Jr., Birch, A. C., & Gizon, L. 2006, ApJ, 646, 553
Duvall, T. L., Jr., Jefferies, S. M., Harvey, J. W., & Pomerantz, M. A. 1993, Nature, 362, 430
Duvall, T. L., Jr., et al. 1997, Sol. Phys., 170, 63
Georgobiani, D., Zhao, J., Kosovichev, A. G., Bensen, D., Stein, R. F., & Nordlund, Å. 2007, ApJ, 657, 1157 (Paper I)
Giles, P. M., Duvall, T. L., Jr., Scherrer, P. H., & Bogart, R. S. 1997, Nature, 390, 52
Gizon, L., & Birch, A. C. 2002, ApJ, 571, 966
Gizon, L., Duvall, T. L., Jr., & Larsen, R. M. 2000, J. Astrophys. Astron., 21, 339
Hindman, B. W., Gizon, L., Duvall, T. L., Jr., Haber, D. A., & Toomre, J. 2004, ApJ, 613, 1253
Hurlburt, N. E., & Rucklidge, A. M. 2000, MNRAS, 314, 793
Jensen, J. M., & Pijpers, F. P. 2003, A&A, 412, 257
Komm, R., Corbard, T., Durney, B. R., González Hernández, I., Hill, F., Howe, R., & Toner, C. 2004, ApJ, 605, 554
Kosovichev, A. G. 1996, ApJ, 461, L55
Kosovichev, A. G., & Duvall, T. L., Jr. 1997, in Proc. SCORe Workshop: Solar Convection and Oscillations and Their Relationship, ed. J. Christensen-Dalsgaard & F. Pijpers (Dordrecht: Kluwer), 241
Kosovichev, A. G., Duvall, T. L., Jr., & Scherrer, P. H. 2000, Sol. Phys., 192, 159
Rickett, J. E., & Claerbout, J. F. 2000, Sol. Phys., 192, 203
Schüssler, M., & Vögler, A. 2006, ApJ, 641, L73
Stein, R. F., & Nordlund, Å. 2000, Sol. Phys., 192, 91
———. 2006, ApJ, 642, 1246
Švanda, M., Zhao, J., & Kosovichev, A. G. 2007, Sol. Phys., DOI: 10.1007/s11207-007-0333-4
Zhao, J., & Kosovichev, A. G. 2003, in Proc. *SOHO* 12/GONG+ Workshop, Local and Global Helioseismology: The Present and Future, ed. H. Sawaya-Lacoste (ESA SP-517; Noordwijk: ESA), 417
———. 2004, ApJ, 603, 776
Zhao, J., Kosovichev, A. G., & Duvall, T. L., Jr. 2001, ApJ, 557, 384